A Physics-Informed Blur Learning Framework for Imaging Systems

Supplementary Material

A. Formula and Concept

A.1. From PSF to SFR

The modulation transfer function (MTF) characterizes the relationship between the point spread function (PSF) and the spatial frequency response (SFR). It is defined as:

$$\mathrm{MTF}(\mathrm{H}, \lambda, \mathbf{f}) = |\mathcal{F}(\mathrm{PSF}(\mathrm{H}, \lambda, \mathbf{x}))|, \tag{A1}$$

where the vector $\mathbf{x} \in \mathbb{R}^2$ is the spatial location on the image plane, λ is the wavelength, and H is normalized field height. The SFR corresponds to a cross-section of the MTF along a specific orientation ϕ, given by:

$$\mathrm{SFR}(\mathrm{H}, \lambda, \phi) = \mathrm{MTF}(\mathrm{H}, \lambda, (-sin\phi, cos\phi) \cdot \mathbf{f}), \tag{A2}$$

where the ϕ is the rotation angle from the +Y axis on the image plane, with positive values indicating clockwise rotation, the vector $\mathbf{f} \in \mathbb{R}^2$ corresponds to the frequency components. For simplify, the SFR can be derived from the PSF as Eqs. (A1) and (A2):

$$\mathrm{SFR}(\mathrm{H}, \lambda, \phi) = h(\mathrm{PSF}(\mathrm{H}, \lambda), \phi), \tag{A3}$$

where h is a mapping function that converts the PSF to the SFR.

A.2. From PSF Shift to Chromatic Aberration Area

Consider an ideal checkerboard pattern with a black-and-white edge at normalized image height H and angular coordinate ϕ, which denotes the rotation angle from the +Y axis on the image plane. Suppose $\mathrm{PSF}^*_{\mathrm{S}}(\mathrm{H}, \lambda, \mathbf{x})$ is shifted PSF after $\mathcal{G}_{\Theta_2}$, this PSF must be rotated by ϕ to align with the edge direction, expressed as:

$$\mathrm{PSF}^*_{\mathrm{R}}(\mathrm{H}, \lambda, \mathbf{x}') = \mathrm{PSF}^*_{\mathrm{S}}(\mathrm{H}, \lambda, R(\phi)\mathbf{x}), \tag{A4}$$

where the new coordinates $\mathbf{x}'$ are:

$$\mathbf{x}' = R(\phi)\mathbf{x}, \tag{A5}$$

and the rotation matrix $R(\phi)$ is given by:

$$R(\phi) = \begin{pmatrix} \cos\phi & \sin\phi \\ -\sin\phi & \cos\phi \end{pmatrix}. \tag{A6}$$

Here, we introduce the edge spread function (ESF) to establish the relationship between the PSF and chromatic aberration. ESF is derived by:

$$\mathrm{ESF}^*(\mathrm{H}, \lambda, \phi) = \int_{x \le \alpha} \int_y \mathrm{PSF}^*_{\mathrm{R}}(\mathrm{H}, \lambda, \mathbf{x})\, dy\, dx. \tag{A7}$$

The chromatic aberration area CA is defined as the integral of the ESF curve:

$$\mathrm{CA}^*(H, \lambda, \phi) = \int_\alpha \mathrm{ESF}^*(H, \lambda, \phi)\, d\alpha. \tag{A8}$$

For simplify, the chromatic aberration area CA can be derived from the PSF:

$$\mathrm{CA}^*(\mathrm{H}, \lambda, \phi) = \mathcal{L}(\mathrm{PSF}^*_{\mathrm{S}}(\mathrm{H}, \lambda, \mathbf{x}), \phi), \tag{A9}$$

where $\mathcal{L}$ is a mapping function from PSF shifts to chromatic aberration.

B. Seidel Basis and Proposed Wavefront Basis

	Seidel Basis	Wavefront Basis	
		cos	sin
1	ρ^2	$\rho^2 \cos\theta^2$	$\rho^2 \sin\theta^2$
2	$\rho^3 \sin\theta$	–	$\rho^3 \sin\theta$
3	$\rho^3 \sin\theta^3$	–	$\rho^3 \sin\theta^3$
4	ρ^4	$\rho^4 \cos\theta^2$	$\rho^4 \sin\theta^2$
5	$\rho^5 \sin\theta$	–	$\rho^5 \sin\theta$
6	ρ^6	$\rho^6 \cos\theta^2$	$\rho^6 \sin\theta^2$

Table A1. Decomposition of Seidel basis into proposed wavefront basis.

As shown in Tab. A1, the wavefront basis is obtained by decomposing the Seidel basis. To fully evaluate the proposed wavefront basis, we compare the results optimized with both the Seidel basis and the proposed wavefront basis. As seen in Fig. A1, the optimization results using the Seidel basis do not provide a high-accuracy estimation.

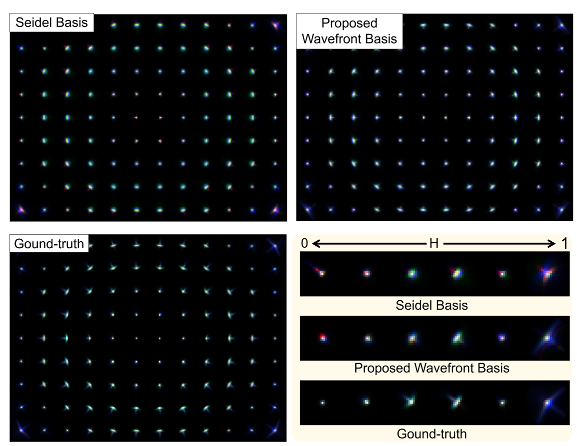

Figure A1. PSF maps of both the estimated and ground-truth data, with PSFs sampled at evenly spaced intervals along the diagonal of the imaging plane (displayed at the bottom-right).

C. Experiments on Real Captures

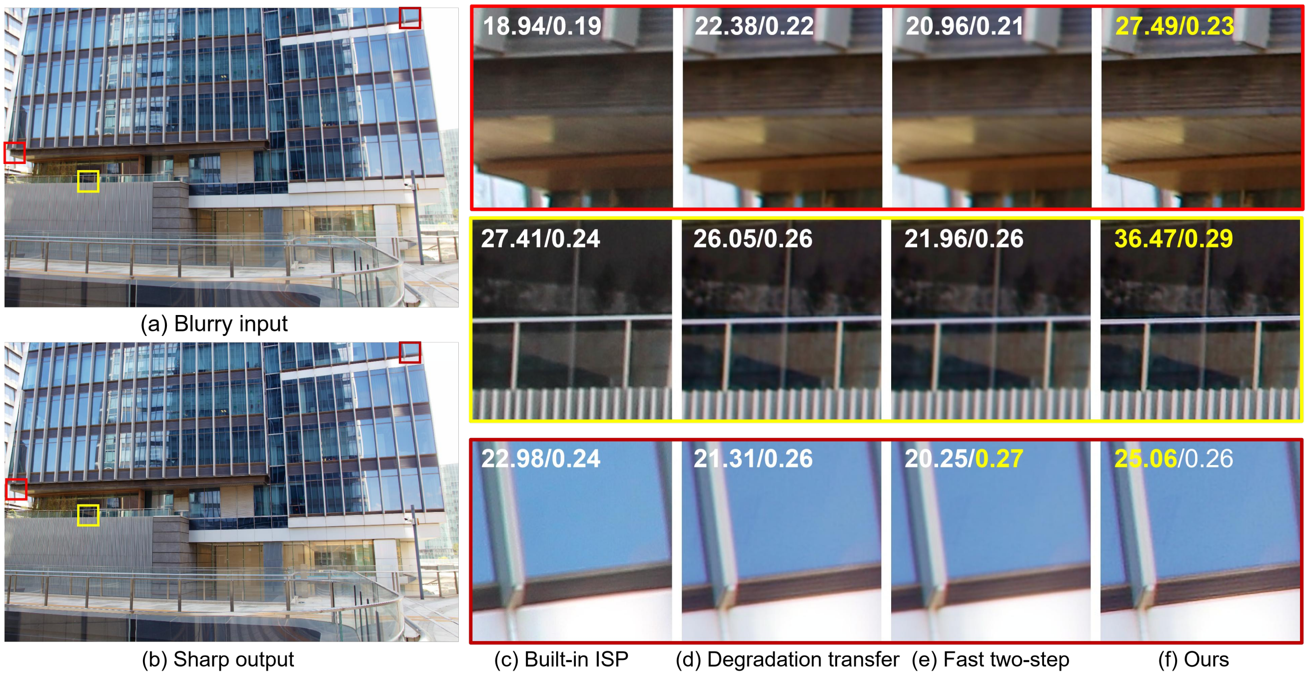

Figure A2. Deblurring comparison results. From (a) to (f): blurry input captured with a Canon EOS600D camera, sharp output by our method, images processed by the built-in ISP, and deblurred images processed separately by Degradation Transfer, Fast Two-step, and our method with Restormer. MUSIQ↑ / MANIQA↑ scores are shown in the top-left corner. As shown, our approach effectively sharpens the image and outperforms the others in terms of MUSIQ and MANIQA scores (higher is better).

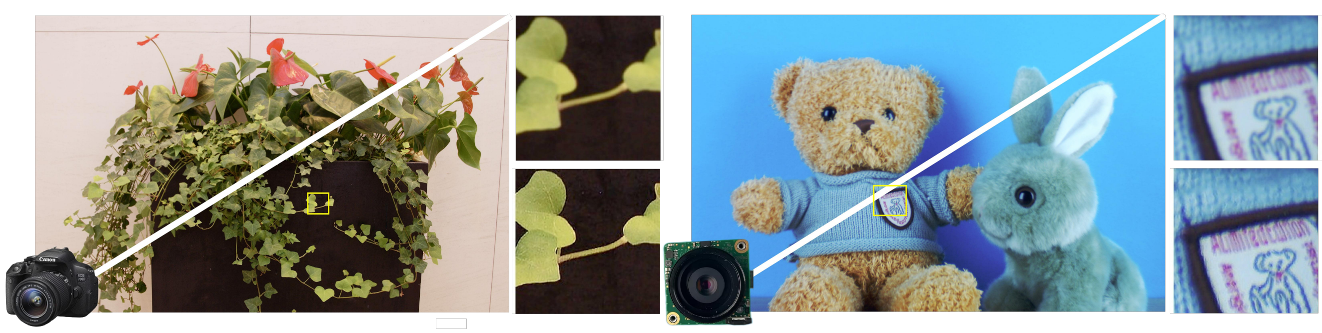

Figure A3. Validation of the proposed blur learning framework on different devices. Restormer is applied to deblur images trained with the estimated PSF. The captured images are shown in the top-left, and the deblurred images in the bottom-right, with patch comparisons displayed on the right (deblurred patches at the bottom). Left: captured with a custom-built device (Edmund lens #63762 and Onsemi AR1820HS sensor); right: captured with a Canon EOS600D. As shown, the deblurred image patches reveal more details.

Figure A4. Deblurring results for an outdoor scene captured with a Canon EOS600D camera. From left to right: sharp output produced by our method, comparison patches (top: captured patches, bottom: patches deblurred by our method using Restormer).

Figure A5. Failure case, chromatic aberrations in the wide field of view remain partially uncorrected.